

# Classifying and harnessing multi-mode light-matter interaction in lossy resonators

Dominik Lentrodt,<sup>1,\*</sup> Oliver Diekmann,<sup>1</sup> Christoph H. Keitel,<sup>1</sup> Stefan Rotter,<sup>2</sup> and Jörg Evers<sup>1,†</sup>

<sup>1</sup>*Max-Planck-Institut für Kernphysik, Saupfercheckweg 1, 69117 Heidelberg, Germany*

<sup>2</sup>*Institute for Theoretical Physics, Vienna University of Technology (TU Wien), 1040 Vienna, Austria*

We develop a practical framework to characterize multi-mode effects on quantum systems coupled to lossy resonators. By relating a generic quantum optical few-mode model to the Mittag-Leffler pole expansion of the cavity’s classical electromagnetic Green’s function, we identify three distinct classes of multi-mode effects in the strong-loss regime. We show that these effects are crucial for understanding spectroscopic signatures in leaky and absorptive resonators, and that they further provide a physical mechanism to design artificial quantum systems through such environments. Both aspects are illustrated using examples in X-ray cavity QED with Mössbauer nuclei.

In the study of quantum matter interacting with the resonant field of a cavity, an important theoretical [1, 2] and experimental paradigm [3, 4] is the coupling to a single cavity mode [5]. More recently, regimes beyond single mode light-matter interaction have moved into the focus of attention. In particular, multi-mode cavity QED has opened new possibilities for many-body quantum systems [6], for example by enabling the tuning of effective interactions [7]. Also for single atoms, qualitatively new dynamics can be realized when multiple modes participate, such as in the multi-mode strong coupling regime [8], where the extreme light-matter coupling bridges the free spectral range between the modes [9].

For many platforms, the realization of extreme coupling strengths or the related mode control remain technically challenging. However, multi-mode features may also appear in the opposite regime of open and absorptive resonators, e.g., if the mode widths exceed their frequency spacing [10]. Interestingly, strong losses do not necessarily represent an obstacle, but may instead cause fascinating phenomena, such as for lasers [11–14] and in the context of non-Hermitian physics [15–19], in general.

However, a systematic understanding of multi-mode light-matter interaction in loss-dominated regimes is currently lacking. For example, in nano-photonics, where complex mode structures can be engineered [20] and losses are often sizable [21], the question of how to describe quantum dynamics in such electromagnetic environments has sparked recent theoretical interest [22, 23]. Another example is the emerging platform of X-ray cavity QED with ensembles of Mössbauer nuclei [24]. It uniquely combines the possibility of high-precision spectroscopy at X-ray energies using the extreme  $Q$ -values of the involved nuclear resonances with cavities which are restricted to the leaky and absorptive regime due to the low refractive index contrast at hard X-ray energies. As a result, single-mode models fail to quantitatively describe the nuclear spectra [25]. A key application of such cavity-nuclei systems is to engineer artificial few-level quantum systems, which are otherwise inaccessible at hard X-ray energies [26–35]. In this case, the properties of the artificial quantum system crucially depend on multi-mode

effects, in a way that is still poorly understood. Similar challenges are encountered in the aforementioned nano-photonics platforms, with potential applications ranging from quantum plasmonics [36] to cavity-controlled chemistry [37, 38].

Here, we develop a framework for identifying, quantifying and interpreting multi-mode effects in loss-dominated regimes of light-matter interaction within structured environments. Our approach is based on relating quantum optical few-mode models to a pole expansion of the classical Green’s function characterizing the electromagnetic environment of a quantum emitter. Using a single two-level atom coupled to a cavity as an example, we identify and quantify three multi-mode mechanisms that lead to qualitative deviations of the spectra from standard single-mode predictions. These results not only crucially affect the interpretation of spectra in the loss-dominated regime. They further offer a mechanism to engineer the quantum emitter’s properties via the loss-induced multi-mode effects to one’s advantage. We illustrate both aspects with examples in X-ray cavity QED, and show that the multi-mode effects allow one to invert the sign of a collective cavity-induced nuclear Lamb shift.

*Single-mode case.*—We start with a single-mode treatment of a generic cavity, see Fig. 1(a). Without atom, the frequency-dependent reflection coefficient is [39]

$$r_{\text{cav}}(\omega) = 1 - 2\pi i \frac{|\kappa_R|^2}{\omega - \omega_1 + i\frac{\kappa}{2}}, \quad (1)$$

where  $\omega$  is the probing light frequency,  $\kappa_R$  the coupling rate in and out of the cavity mode of frequency  $\omega_1$ , and  $\kappa$  the total cavity loss rate. We denote the relevant minimum in this empty-cavity reflectance ( $|r_{\text{cav}}|^2$ ) as  $\omega_{\text{min}}$ , which in the single-mode case coincides with  $\omega_1$ . An example reflectance (featuring multiple modes) is shown in Fig. 1(b). Coupling a single two-level atom with rate  $g$  near-resonantly to the cavity mode leads to the famous Jaynes-Cummings (JC) model [1]. At weak mode-atom coupling, the linear reflection spectrum becomes [39]

$$r(\omega) \approx r_{\text{cav}}(\omega_a) - 2\pi i \frac{(\kappa_R^{\text{(int)}})^2}{\omega - \omega_a - \Delta + i\Gamma/2}, \quad (2)$$

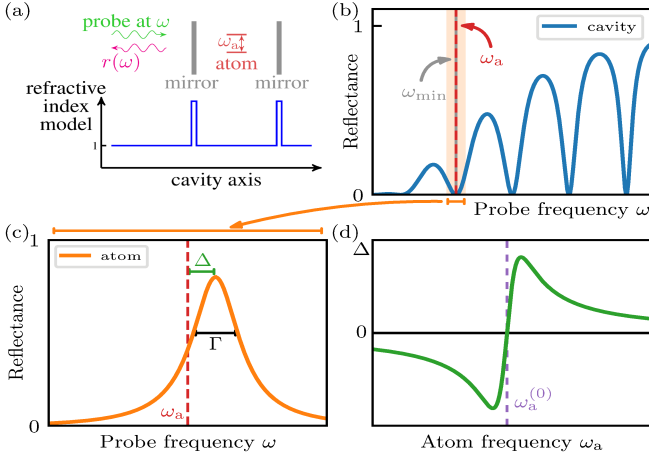


FIG. 1. Model setup and the spectroscopic quantities considered in the analysis. (a) Model cavity coupled to a two-level atom at its center. The system is probed via its reflectance  $|r(\omega)|^2$ . (b) Reflectance for the case of spectrally broad cavity modes and a narrow atomic resonance. (c) shows a magnification of (b) around the atomic resonance, from which a frequency shift  $\Delta$  and a line broadening  $\Gamma$  of the resonance can be extracted. (d) The cavity-induced Lamb shift  $\Delta$  as a function of the atomic transition frequency  $\omega_a$ . We denote the location of its zero crossing as  $\omega_a^{(0)}$ .

where the resonance modulation depth is given by  $(\kappa_R^{(\text{int})})^2 = |\kappa_R g|^2 / (\omega_a - \omega_1 + i\kappa/2)^2$ . The real-valued cavity-induced Lamb shift  $\Delta$  and the Purcell broadened atomic resonance line width  $\Gamma$  [40] define together a complex level shift

$$\delta := \Delta - i\frac{\Gamma}{2} = \frac{gg^*}{\omega_a - \omega_1 + i\frac{\kappa}{2}}, \quad (3)$$

which can be extracted from the reflection spectrum, see Fig. 1(c). Subsequently, one can analyze these parameters as a function of the atomic transition frequency  $\omega_a$ , which in the single-mode case results in a dispersion-like shape for  $\Delta$  as shown in Fig. 1(d). We denote the atomic resonance frequency at which  $\Delta = 0$  as  $\omega_a^{(0)}$ .

By inspection of Eqs. (1)-(3), we find that the minimum of the empty cavity reflectance  $\omega_{\min}$ , the zero of the frequency shift  $\Delta(\omega_a^{(0)}) = 0$ , the maximum of the line width broadening  $\Gamma$ , and the real part  $\omega_1$  of the pole location of  $\Delta(\omega)$  in the complex frequency plane all coincide at the cavity mode frequency  $\omega_{\min} = \omega_a^{(0)} = \omega_1$ . This frequency coincidence of all key spectroscopic features renders the interpretation of spectroscopic data straightforward. However, it also severely impedes the design of the system properties, since only the detuning between atom and cavity, the cavity loss rate, and the reflection out-coupling remain as control parameters. For example, the light-matter coupling rate  $g$  simply scales the energy shift and line broadening. As one consequence, single-mode cavity models do not allow for non-zero shifts  $\Delta$  at

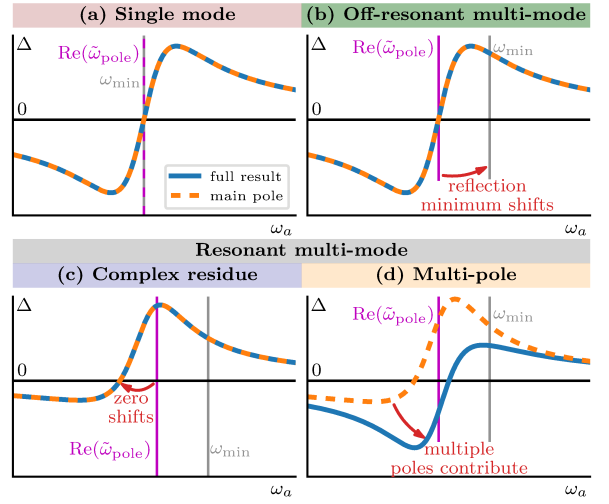


FIG. 2. Classification of multi-mode effects, illustrated via the Lamb shift  $\Delta$  close to the atomic resonance as in Fig. 1(d). (a) Single-mode case. The main pole in Eq. (6) is sufficient, and the cavity resonance  $\omega_1 = \text{Re}(\tilde{\omega}_{\text{pole}})$ , the reflectance minimum  $\omega_{\min}$  and the zero of  $\Delta$  at  $\omega_a^{(0)}$  coincide. (b) Off-resonant multi-mode effects can appear already in the empty-cavity reflectance, and lift the degeneracy of  $\text{Re}(\tilde{\omega}_{\text{pole}})$  and  $\omega_{\min}$ . (c, d) Resonant multi-mode effects, which affect the light-matter interaction. (c) In the complex-residue case, the main pole residue has an imaginary contribution, unlike in the single mode case. This shifts the zero  $\omega_a^{(0)}$  of  $\Delta$  from  $\omega_{\min}$ , and modifies the shape of  $\Delta(\omega_a)$ . (d) In the multi-pole case, more than one pole is required for convergence.

the minimum  $\omega_{\min}$  of the cavity background  $r_{\text{cav}}$ , which is at odds with the experimental observation of a non-zero shift at the cavity resonance reported in Fig. 3 of [26]. Motivated by this, we focus the following discussion on the Lamb shift  $\Delta$  as an observable.

*Multi-mode case.*—Next, we generalize to the multi-mode case. We employ a recently developed few-mode model applicable to general complex and absorptive resonators [22, 39], given by the Master equation

$$\dot{\rho} = -i[H; \rho] + \sum_i \frac{\kappa_i}{2} \left( 2\hat{a}_i \rho \hat{a}_i^\dagger - \hat{a}_i^\dagger \hat{a}_i \rho - \rho \hat{a}_i^\dagger \hat{a}_i \right), \quad (4)$$

where  $H = H_{\text{cav}} + H_{\text{atom}}$ , with an interacting cavity mode Hamiltonian  $H_{\text{cav}} = \sum_{ij} \omega_{ij} \hat{a}_i^\dagger \hat{a}_j$ , and the JC Hamiltonian  $H_{\text{atom}} = (\omega_a/2)\hat{\sigma}^z + \sum_i [g_i^* \hat{a}_i \hat{\sigma}^+ + h.c.]$ . Equation (3) then generalizes to [39, 41]

$$\delta = \underline{g}^\dagger \left[ \omega_a - \underline{\omega}_{\text{cav}} + \frac{i}{2} \underline{\kappa} \right]^{-1} \underline{g}, \quad (5)$$

where  $(\underline{g})_i = g_i$ ,  $(\underline{\omega}_{\text{cav}})_{ij} = \omega_{ij}$  and  $(\underline{\kappa})_{ij} = \kappa_i \delta_{ij}$  are the multi-mode couplings, cavity mode interactions and decay terms, respectively, in matrix-vector notation.

*From multi-mode models to pole expansions.*— In order to certify and categorize multi-mode effects, we diagonal-

ize Eq. (5) as

$$\delta = \sum_i \frac{\tilde{g}_i^* \tilde{g}_i}{\omega_a - \tilde{\Omega}_i + i \frac{\tilde{\kappa}_i}{2}}, \quad (6)$$

where the diagonal basis parameters relate to the bare mode parameters in Eq. (5) by an invertible transformation matrix [39]. In practice, the bare mode parameters often are obtained by a fitting procedure [22]. Instead, we express the level shift in terms of the cavity's classical Green's function  $\mathbf{G}$  as  $\delta = -\mu_0 \omega_a^2 \mathbf{d}^* \cdot \mathbf{G}(\mathbf{r}_a, \mathbf{r}_a, \omega_a) \cdot \mathbf{d}$  [42–45] where  $\mathbf{d}$  is the transition's dipole moment vector, and expand  $\mathbf{G}$  using a Mittag-Leffler (ML) pole expansion as [10, 39, 46, 47]

$$\delta = \sum_i \frac{r_i}{\omega_a - \tilde{\omega}_{\text{pole},i}}. \quad (7)$$

A comparison of Eqs. (6,7) shows that one can extract the complex pole frequencies  $\tilde{\omega}_{\text{pole},i} = \tilde{\Omega}_i - i \tilde{\kappa}_i/2$  and their residues  $r_i = \tilde{g}_i^* \tilde{g}_i$  of the multi-mode model directly from the Green's function of the resonator system, without the need for fitting. Note that here we assumed that the diagonalization exists and comprises only simple poles. A more general treatment is required, e.g., in the presence of exceptional points [16, 17].

A key feature of our approach is that the ML expansion is unique and independent of any modal basis choice. Therefore, its truncation to a variable number of poles around  $\omega_a$  can be used to certify and categorize multi-mode effects via the breakdown of characteristic features in the single-mode case discussed above.

*Classification of multi-mode effects.*— By comparison to the single mode formula Eq. (3), we find that three conditions on the pole expansion Eqs. (6,7) have to be fulfilled for a single-mode scenario. A violation of any of these conditions renders the single-mode treatment invalid, thereby implying three different classes of multi-mode effects. We illustrate these effects by their action on the cavity-induced frequency shift  $\Delta$  as a function of the atomic resonance frequency  $\omega_a$  in Fig. 2. In each panel, the result after inclusion of each effect beyond the single mode case is compared to the corresponding fully converged multi-mode result.

In the single-mode case (a), already the main pole is sufficient for a quantitative description, with the aforementioned frequency coincidence  $\omega_a^{(0)} = \text{Re}(\tilde{\omega}_{\text{pole}}) = \omega_{\text{min}}$ .

The first condition for the single-mode case is that a single main pole has to be sufficient in a relevant frequency range covering the atomic line width to achieve convergence of the ML expansion. The opposite case, where multiple poles are required for good convergence, we will refer to as a *multi-pole effect*, see Fig. 2(d).

Second, we also require real-valued residues, since the residue  $|g|^2$  in the single-mode case Eq. (3) is real. *Complex-residue effects* appear if the main pole  $\tilde{\omega}_{\text{pole}}$  has

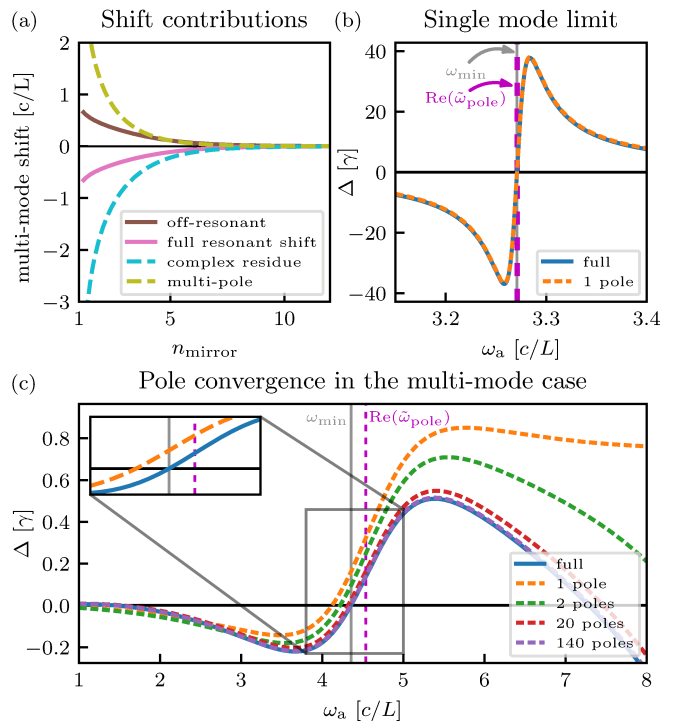


FIG. 3. Transition from the single-mode to the multi-mode case in Fabry-Pérot-like cavities, controlled by the barrier refractive index  $n_{\text{mirror}}$ . Panel (a) quantifies the resonant multi-mode effects via the displacement of the zero of  $\Delta$  from the position  $\text{Re}(\tilde{\omega}_{\text{pole}})$  of the main pole. Contributions of complex-residue and multi-pole effects are shown separately (see legend). The solid brown line indicates the off-resonant shift  $\text{Re}(\tilde{\omega}_{\text{pole}}) - \omega_{\text{min}}$  for comparison. (b) Cavity-induced energy shift  $\Delta$  in the single-mode limit ( $n_{\text{mirror}} = 20$ ). (c) Corresponding results in a multi-mode case ( $n_{\text{mirror}} = 4$ ), where multiple poles are required to achieve convergence, and even the single-pole line shape differs from the single-mode case due to complex residue effects. The inset shows the full and single-pole results around the pole location to make their shifts visible. In panels (b,c), the vertical black lines show the minimum  $\omega_{\text{min}}$  of the empty cavity reflectance, while the magenta dashed line shows the position  $\text{Re}(\tilde{\omega}_{\text{pole}})$  of the main pole.  $\gamma$  is the free space radiative line width.

a non-negligible imaginary part of its residue. Then, already the first pole contribution to the shape of  $\Delta(\omega_a)$  is modified and its zero  $\omega_a^{(0)}$  moves away from the pole location  $\text{Re}(\tilde{\omega}_{\text{pole}})$ , see Fig. 2(c).

Both complex-residue and multi-pole effects are *resonant effects*, since they directly affect the cavity-modified properties  $\Delta$  and  $\Gamma$  of the atom, and *multi-mode effects*, since the single-mode JC model fails to capture them. However, single-mode models may fail even in the absence of the atom, if the empty-cavity reflectance deviates from its single-mode form Eq. (1) due to spectral overlap between cavity modes. These *off-resonant multi-mode effects* typically shift the pole and therefore the zero  $\omega_a^{(0)}$  of  $\Delta$  away from the minimum  $\omega_{\text{min}}$  of the empty-cavity

reflectance [25], see Fig. 2(b). We note that a natural interpretation for the multi-mode effects can also be given in terms of the multi-mode cavity model Eq. (4) [39].

*Multi-mode effects in Fabry-Pérot-like cavities.*—Next, we explore the relevance of the different multi-mode effects by analyzing a simple model reminiscent of archetype Fabry-Pérot cavities, see Fig. 1(a). The cavity of length  $L$  is modeled via a piece-wise constant one-dimensional refractive index comprising vacuum with two mirror layers of refractive index  $n_{\text{mirror}}$  and thickness  $t_{\text{mirror}} = L/100$ . Note that  $n_{\text{mirror}}$  here merely acts as a model parameter with unrealistically high values, while in practice highly reflecting mirrors comprise multi-layer dielectrics [3]. This model allows us to study the continuous transition between the single and multi-mode case by inducing spectral mode overlap via high leakage through the mirrors.

Results are shown in Fig. 3. Panel (a) quantifies resonant multi-mode effects via the displacement of the zero  $\omega_a^{(0)}$  of  $\Delta(\omega_a)$  from the main pole position  $\text{Re}(\tilde{\omega}_{\text{pole}})$  as a function of  $n_{\text{mirror}}$ , and off-resonant multi-mode effects via the shift of  $\text{Re}(\tilde{\omega}_{\text{pole}})$  from  $\omega_{\text{min}}$ . For the single-mode case in high-quality resonators with well-isolated resonances ( $n_{\text{mirror}} \gg 1$ ), all shifts vanish. As expected, towards lower-quality resonators, the multi-mode effects become more and more relevant. Interestingly, the large negative complex-residue shift is partially canceled by the multi-pole and off-resonant shifts in this cavity. Panels (b,c) show  $\Delta$  as a function of the atomic transition frequency  $\omega_a$  for a single-mode (b,  $n_{\text{mirror}} = 20$ ) and a multi-mode (c,  $n_{\text{mirror}} = 4$ ) scenario. As expected, in the single-mode case, one pole is sufficient to model the system, and no zero-shift of  $\Delta$  appears. In contrast, the multi-mode case in (c) requires many poles for convergence, has a non-vanishing zero-shift of  $\Delta$  from the pole due to resonant multi-mode effects, and features line-shape modifications due to the complex-residue effect. The single-pole approximation clearly deviates from the full result and has a significantly complex residue. These observations are incompatible with the single-mode model Eqs. (1)-(3).

*Multi-mode level shift design.*—Finally, we explore the multi-mode effects outlined above in the concrete platform of thin-film X-ray cavity QED with Mössbauer nuclei, which has recently attracted considerable theoretical [25, 32, 34, 35, 48, 49] and experimental [26–31, 50] attention. Similar setups with electronic processes are starting to be explored [51–53]. In these cavities, the atom is replaced by a thin layer containing an ensemble of Mössbauer nuclei. Because of the low refractive-index contrast, the cavities are generally loss-dominated and probed in grazing incidence. In the experimentally relevant low-excitation regime [34], the cavity-nuclei system can be approximated as a few-level quantum system [32, 39], comprising the collective ground state and excitonic single-excitation states coherently spread over

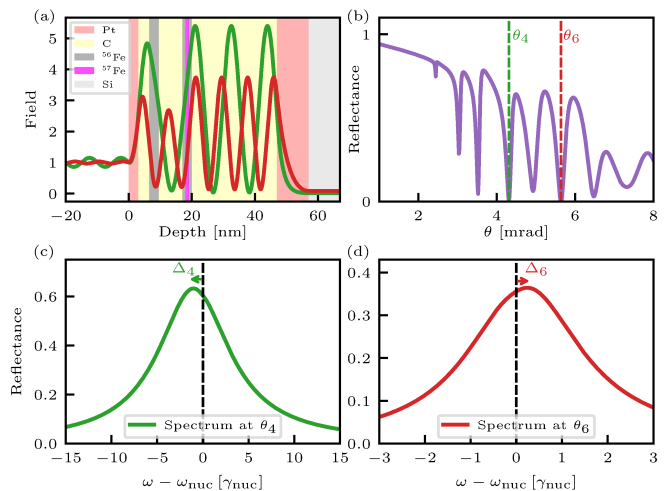


FIG. 4. Design of multi-mode level shifts. (a) Cavity geometry and off-resonant field distributions in the fourth ( $\theta_4$ , green) and sixth ( $\theta_6$ , red) cavity mode. The cavity structure is Pt (3 nm)/C (3.5 nm)/<sup>56</sup>Fe (3 nm)/C (7.5 nm)/<sup>56</sup>Fe (1 nm)/<sup>57</sup>Fe (1 nm)/<sup>56</sup>Fe (1 nm)/C (27 nm)/Pt (10 nm)/Si. (b) Off-resonant cavity reflectance as function of incidence angle showing the overlapping mode structure. Both, the fourth and the sixth mode are critically coupled. (c,d) Nuclear spectra at  $\theta_4, \theta_6$ , demonstrating the reversed energy shift in the two mode minima.

the nuclei. Such cavities thus form a promising platform to implement quantum optical schemes at hard X-ray energies, which are otherwise unavailable due to the lack of suitable X-ray driving fields. For this purpose, the possibility to control the quantum optical parameters is key to implement more advanced quantum optical level schemes [24, 33]. From an experimental point of view, operation in critical coupling at a minimum of the empty-cavity reflectance  $\omega_{\text{min}}$  is highly desirable, in order to suppress the strong and spectrally broad electronic scattering background. However, in this latter case, the single-mode case severely impedes the parameter control, as discussed below Eqs. (1)-(3).

The calculations in Fig. 4 show that the above-developed multi-mode effects provide a physical mechanism to overcome this challenge. The cavity structure shown in panel (a) features overlapping cavity resonances visible in the off-resonant cavity reflectance shown in (b). Panels (c,d) show the resulting spectra of the nuclear resonances for the two modes  $\theta_4$  and  $\theta_6$ , resonantly driven at the respective  $\omega_{\text{min}}$ , and operated in critical coupling. The cavity structure is designed such that the multi-mode effects lead to opposite signs of the respective nuclear Lamb shifts  $\Delta$ . This demonstrates that tuning the mode environment through the cavity geometry allows one to deliberately alter the effective level scheme of the nuclear ensemble in a qualitative way, as it is required, e.g., to satisfy delicate detuning conditions in more complex multi-level systems [54]. A closer inspection [39]

shows that the fourth mode in this cavity mainly features off-resonant multi-mode effects, while the sixth mode is strongly influenced by resonant multi-mode effects. An analogous analysis [39] reveals that already the first experimental observation of the collective Lamb shift in a similar cavity [26] relies on an off-resonant multi-mode effect, illustrating the importance for the interpretation of spectroscopic observables.

*Conclusion.*—In summary, we have presented a simple method to identify and classify multi-mode effects on the quantum properties of a two-level system in resonators with losses and complex spectra. These effects are not only crucial for the interpretation of spectroscopic observables in loss-dominated regimes. They also provide a new physical mechanism to tune quantum systems by understanding and harnessing multi-mode effects in lossy resonators, connecting quantum optical concepts to recent suggestions from non-Hermitian photonics [16]. We exemplified the resulting possibilities to control quantum optical parameters by exploiting multi-mode effects on an artificial X-ray few-level system to invert its Lamb shift compared to observations in previous experiments [26]. The systematic design of such multi-mode cavity environments [55] provides a clear path towards the implementation of more complex quantum optical multi-level systems at hard X-ray energies, paving the way for a multitude of applications. Together with new source technology [56], we envision, in particular, the study of as-yet unexplored non-linear interactions between X-rays and nuclei, via the deliberate design of few-level schemes that may coherently enhance non-linear susceptibilities [54].

The authors would like to thank L. Bocklage and K. P. Heeg for valuable discussions. OD gratefully acknowledges support by the Cusanuswerk and the Studienstiftung des deutschen Volkes.

---

\* dominik.lentrodt@mpi-hd.mpg.de

† joerg.evers@mpi-hd.mpg.de

- [1] E. T. Jaynes and F. W. Cummings, *Comparison of quantum and semiclassical radiation theories with application to the beam maser*, Proc. IEEE **51**, 89 (1963).
- [2] P. Kirton, M. M. Roses, J. Keeling, and E. G. Dalla Torre, *Introduction to the dicke model: From equilibrium to nonequilibrium, and vice versa*, Advanced Quantum Technologies **2**, 1800043 (2019).
- [3] S. Haroche and J. M. Raimond, *Exploring the Quantum: Atoms, Cavities, and Photons* (Oxford Univ. Press, Oxford, 2006).
- [4] A. Kavokin, J. J. Baumberg, G. Malpuech, and F. P. Laussy, *Microcavities* (Oxford University Press, 2017).
- [5] D. O. Krimer, S. Putz, J. Majer, and S. Rotter, *Non-markovian dynamics of a single-mode cavity strongly coupled to an inhomogeneously broadened spin ensemble*, Phys. Rev. A **90**, 043852 (2014).
- [6] H. Ritsch, P. Domokos, F. Brennecke, and T. Esslinger, *Cold atoms in cavity-generated dynamical optical potentials*, Rev. Mod. Phys. **85**, 553 (2013).
- [7] V. D. Vaidya, Y. Guo, R. M. Kroeze, K. E. Ballantine, A. J. Kollár, J. Keeling, and B. L. Lev, *Tunable-range, photon-mediated atomic interactions in multimode cavity QED*, Phys. Rev. X **8**, 011002 (2018).
- [8] D. O. Krimer, M. Liertzer, S. Rotter, and H. E. Türeci, *Route from spontaneous decay to complex multimode dynamics in cavity QED*, Phys. Rev. A **89**, 033820 (2014).
- [9] A. Johnson, M. Blaha, A. E. Ulanov, A. Rauschenbeutel, P. Schneeweiss, and J. Volz, *Observation of collective superstrong coupling of cold atoms to a 30-m long optical resonator*, Phys. Rev. Lett. **123**, 243602 (2019).
- [10] P. Lalanne, W. Yan, K. Vynck, C. Sauvan, and J.-P. Hugonin, *Light interaction with photonic and plasmonic resonances*, Laser & Photonics Reviews **12**, 1700113 (2018).
- [11] G. Hackenbroich, C. Viviescas, and F. Haake, *Field quantization for chaotic resonators with overlapping modes*, Phys. Rev. Lett. **89**, 083902 (2002).
- [12] H. Hodaei, M.-A. Miri, M. Heinrich, D. N. Christodoulides, and M. Khajavikhan, *Parity-time-symmetric microring lasers*, Science **346**, 975 (2014).
- [13] B. Peng, Ş. K. Özdemir, S. Rotter, H. Yilmaz, M. Liertzer, F. Monifi, C. M. Bender, F. Nori, and L. Yang, *Loss-induced suppression and revival of lasing*, Science **346**, 328 (2014).
- [14] P. Miao, Z. Zhang, J. Sun, W. Walasik, S. Longhi, N. M. Litchinitser, and L. Feng, *Orbital angular momentum microlaser*, Science **353**, 464 (2016).
- [15] F.-M. Dittes, *The decay of quantum systems with a small number of open channels*, Phys. Rep. **339**, 215 (2000).
- [16] R. El-Ganainy, K. G. Makris, M. Khajavikhan, Z. H. Musslimani, S. Rotter, and D. N. Christodoulides, *Non-hermitian physics and PT symmetry*, Nat. Phys. **14**, 11 (2018).
- [17] M.-A. Miri and A. Alù, *Exceptional points in optics and photonics*, Science **363** (2019), 10.1126/science.aar7709.
- [18] L. Feng, R. El-Ganainy, and L. Ge, *Non-hermitian photonics based on parity-time symmetry*, Nature Photonics **11**, 752 (2017).
- [19] S. Longhi, *Parity-time symmetry meets photonics: A new twist in non-hermitian optics*, EPL (Europhysics Letters) **120**, 64001 (2017).
- [20] P. Peng, Y.-C. Liu, D. Xu, Q.-T. Cao, G. Lu, Q. Gong, and Y.-F. Xiao, *Enhancing coherent light-matter interactions through microcavity-engineered plasmonic resonances*, Phys. Rev. Lett. **119**, 233901 (2017).
- [21] R. Liu, Z.-K. Zhou, Y.-C. Yu, T. Zhang, H. Wang, G. Liu, Y. Wei, H. Chen, and X.-H. Wang, *Strong light-matter interactions in single open plasmonic nanocavities at the quantum optics limit*, Phys. Rev. Lett. **118**, 237401 (2017).
- [22] I. Medina, F. J. García-Vidal, A. I. Fernández-Domínguez, and J. Feist, *Few-mode field quantization of arbitrary electromagnetic spectral densities*, Phys. Rev. Lett. **126**, 093601 (2021).
- [23] S. Franke, S. Hughes, M. K. Dezfouli, P. T. Kristensen, K. Busch, A. Knorr, and M. Richter, *Quantization of quasinormal modes for open cavities and plasmonic cavity quantum electrodynamics*, Phys. Rev. Lett. **122**, 213901 (2019).

- [24] R. Röhlsberger and J. Evers, Quantum optical phenomena in nuclear resonant scattering, in *Modern Mössbauer Spectroscopy*, edited by Y. Yoshida and G. Langouche (Springer Singapore, Singapore, 2021) pp. 105–171.
- [25] K. P. Heeg and J. Evers, *Collective effects between multiple nuclear ensembles in an x-ray cavity-QED setup*, Phys. Rev. A **91**, 063803 (2015).
- [26] R. Röhlsberger, K. Schlage, B. Sahoo, S. Couet, and R. Rüffer, *Collective lamb shift in single-photon superradiance*, Science **328**, 1248 (2010).
- [27] R. Röhlsberger, H.-C. Wille, K. Schlage, and B. Sahoo, *Electromagnetically induced transparency with resonant nuclei in a cavity*, Nature **482**, 199 (2012).
- [28] K. P. Heeg, H.-C. Wille, K. Schlage, T. Guryeva, D. Schumacher, I. Uschmann, K. S. Schulze, B. Marx, T. Kämpfer, G. G. Paulus, R. Röhlsberger, and J. Evers, *Vacuum-assisted generation and control of atomic coherences at x-ray energies*, Phys. Rev. Lett. **111**, 073601 (2013).
- [29] K. P. Heeg, J. Haber, D. Schumacher, L. Bocklage, H.-C. Wille, K. S. Schulze, R. Loetzsch, I. Uschmann, G. G. Paulus, R. Rüffer, R. Röhlsberger, and J. Evers, *Tunable subluminal propagation of narrow-band x-ray pulses*, Phys. Rev. Lett. **114**, 203601 (2015).
- [30] J. Haber, K. S. Schulze, K. Schlage, R. Loetzsch, L. Bocklage, T. Guryeva, H. Bernhardt, H.-C. Wille, R. Rüffer, I. Uschmann, G. G. Paulus, and R. Röhlsberger, *Collective strong coupling of x-rays and nuclei in a nuclear optical lattice*, Nat. Phot. **10**, 445 EP (2016).
- [31] J. Haber, X. Kong, C. Strohm, S. Willing, J. Gollwitzer, L. Bocklage, R. Rüffer, A. Pálffy, and R. Röhlsberger, *Rabi oscillations of x-ray radiation between two nuclear ensembles*, Nat. Phot. **11**, 720 (2017).
- [32] K. P. Heeg and J. Evers, *X-ray quantum optics with mössbauer nuclei embedded in thin-film cavities*, Phys. Rev. A **88**, 043828 (2013).
- [33] P. Longo, C. H. Keitel, and J. Evers, *Tailoring superradiance to design artificial quantum systems*, Scientific Reports **6**, 23628 (2016).
- [34] D. Lentrodt, K. P. Heeg, C. H. Keitel, and J. Evers, *Ab initio quantum models for thin-film x-ray cavity qed*, Phys. Rev. Research **2**, 023396 (2020).
- [35] X. Kong, D. E. Chang, and A. Pálffy, *Green's-function formalism for resonant interaction of x rays with nuclei in structured media*, Phys. Rev. A **102**, 033710 (2020).
- [36] M. S. Tame, K. R. McEnery, S. K. Özdemir, J. Lee, S. A. Maier, and M. S. Kim, *Quantum plasmonics*, Nature Physics **9**, 329 (2013).
- [37] R. F. Ribeiro, L. A. Martínez-Martínez, M. Du, J. Campos-Gonzalez-Angulo, and J. Yuen-Zhou, *Polariton chemistry: controlling molecular dynamics with optical cavities*, Chem. Sci. **9**, 6325 (2018).
- [38] J. Feist, J. Galego, and F. J. Garcia-Vidal, *Polaritonic chemistry with organic molecules*, ACS Photonics **5**, 205 (2018), <https://doi.org/10.1021/acsp Photonics.7b00680>.
- [39] See Supplemental Material at XXXX for details on the open single-mode Jaynes-Cummings model, on the Mittag-Leffler expansion of the complex level shift, on its relation to quantum optical few-mode models, and on multi-mode effects in X-ray cavity QED.
- [40] T. Wu, M. Gurioli, and P. Lalanne, *Nanoscale light confinement: the q's and v's*, ACS Photonics **8**, 1522 (2021), <https://doi.org/10.1021/acsp Photonics.1c00336>.
- [41] D. Lentrodt and J. Evers, *Ab initio few-mode theory for quantum potential scattering problems*, Phys. Rev. X **10**, 011008 (2020).
- [42] H. T. Dung, L. Knöll, and D.-G. Welsch, *Spontaneous decay in the presence of dispersing and absorbing bodies: General theory and application to a spherical cavity*, Phys. Rev. A **62**, 053804 (2000).
- [43] S. Scheel and S. Y. Buhmann, *Macroscopic quantum electrodynamics - concepts and applications*, Acta Phys. Slovaca **58**, 675 (2008).
- [44] S. Y. Buhmann and D.-G. Welsch, *Casimir-polder forces on excited atoms in the strong atom-field coupling regime*, Phys. Rev. A **77**, 012110 (2008).
- [45] A. Asenjo-Garcia, J. D. Hood, D. E. Chang, and H. J. Kimble, *Atom-light interactions in quasi-one-dimensional nanostructures: A green's-function perspective*, Phys. Rev. A **95**, 033818 (2017).
- [46] J. Defrance and T. Weiss, *On the pole expansion of electromagnetic fields*, Opt. Express **28**, 32363 (2020).
- [47] T. Wu, D. Arrivault, M. Duruflé, A. Gras, F. Binkowski, S. Burger, W. Yan, and P. Lalanne, *Efficient hybrid method for the modal analysis of optical microcavities and nanoresonators*, J. Opt. Soc. Am. A **38**, 1224 (2021).
- [48] K. P. Heeg, C. H. Keitel, and J. Evers, *Inducing and detecting collective population inversions of mössbauer nuclei*, (2016), arXiv:1607.04116 [quant-ph].
- [49] X. Kong and A. Pálffy, *Stopping narrow-band x-ray pulses in nuclear media*, Phys. Rev. Lett. **116**, 197402 (2016).
- [50] K. P. Heeg, C. Ott, D. Schumacher, H.-C. Wille, R. Röhlsberger, T. Pfeifer, and J. Evers, *Interferometric phase detection at x-ray energies via fano resonance control*, Phys. Rev. Lett. **114**, 207401 (2015).
- [51] J. Haber, J. Gollwitzer, S. Francoual, M. Tolkiehn, J. Strempler, and R. Röhlsberger, *Spectral control of an x-ray l-edge transition via a thin-film cavity*, Phys. Rev. Lett. **122**, 123608 (2019).
- [52] B. Gu, A. Nenov, F. Segatta, M. Garavelli, and S. Mukamel, *Manipulating core excitations in molecules by x-ray cavities*, Phys. Rev. Lett. **126**, 053201 (2021).
- [53] M. Vassholz and T. Salditt, *Observation of electron-induced characteristic x-ray and bremsstrahlung radiation from a waveguide cavity*, Science Advances **7** (2021), 10.1126/sciadv.abd5677.
- [54] M. Fleischhauer, A. Imamoglu, and J. P. Marangos, *Electromagnetically induced transparency: Optics in coherent media*, Rev. Mod. Phys. **77**, 633 (2005).
- [55] O. Diekmann, D. Lentrodt, and J. Evers, *Inverse design of artificial two-level systems with mössbauer nuclei in thin-film cavities*, (2021), arXiv:2108.01960 [quant-ph].
- [56] A. I. Chumakov, A. Q. R. Baron, I. Sergueev, C. Strohm, O. Leupold, Y. Shvyd'ko, G. V. Smirnov, R. Rüffer, Y. Inubushi, M. Yabashi, K. Tono, T. Kudo, and T. Ishikawa, *Superradiance of an ensemble of nuclei excited by a free electron laser*, Nat. Phys. **14**, 261 (2018).

# Classifying and harnessing multi-mode light-matter interaction in lossy resonators

## Supplemental Material

Dominik Lentrodt,<sup>1,\*</sup> Oliver Diekmann,<sup>1</sup> Christoph H. Keitel,<sup>1</sup> Stefan Rotter,<sup>2</sup> and Jörg Evers<sup>1,†</sup>

<sup>1</sup>*Max-Planck-Institut für Kernphysik, Saupfercheckweg 1, 69117 Heidelberg, Germany*

<sup>2</sup>*Institute for Theoretical Physics, Vienna University of Technology (TU Wien), 1040 Vienna, Austria*

This supplemental material provides details on the open single-mode Jaynes-Cummings model, the construction of the quantum optical few-mode expansion of the complex level shift, its relation to the Mittag-Leffler expansion, and further analyzes the multi-mode effects in the x-ray cavity QED example in the main text.

### I. THE OPEN SINGLE MODE JAYNES-CUMMINGS MODEL

In this supplement, we review the standard case of a single mode cavity [S1, S2] containing a two-level system, and derive Eqs. (1)-(3) in the main text. The open single mode Jaynes-Cummings model is given by the Master equation and Hamiltonian [S2]

$$\dot{\rho} = -i[H; \rho] + \frac{\kappa}{2} (2\hat{a}\rho\hat{a}^\dagger - \hat{a}^\dagger\hat{a}\rho - \rho\hat{a}^\dagger\hat{a}), \quad (\text{S1})$$

$$H = \omega_1\hat{a}^\dagger\hat{a} + \frac{\omega_a}{2}\hat{\sigma}^z + \sum_i [g^*\hat{a}\hat{\sigma}^+ + h.c.]. \quad (\text{S2})$$

Here,  $\omega_1$  is the cavity mode's resonance frequency,  $\kappa$  is its decay rate,  $\omega_a$  is the transition frequency of the two-level atom,  $g$  is the mode-atom coupling strength, and  $\hat{a}$  ( $\hat{\sigma}^{z/\pm}$ ) denotes the operator(s) associated with the cavity mode (two-level atom). We note that additional direct loss channels from the atom could easily be added to the model, but we omit them here for simplicity. We use units of  $\hbar = 1$  for the Hamiltonian.

The level shift of the atom is a weak coupling notion, where the cavity acts as a Markovian environment for the atom. In the above model, we can extract it by adiabatically eliminating the cavity mode (see, e.g., [S3]). The resulting atom's Master equation is given by

$$\dot{\rho}_a = -i[H_{\text{adiab}}; \rho_a] + \frac{\Gamma}{2} (2\hat{\sigma}^- \rho_a \hat{\sigma}^+ - \hat{\sigma}^+ \hat{\sigma}^- \rho_a - \rho_a \hat{\sigma}^+ \hat{\sigma}^-), \quad (\text{S3})$$

$$H_{\text{adiab}} = \frac{1}{2}(\omega_a + \Delta)\hat{\sigma}^z. \quad (\text{S4})$$

The cavity-induced frequency shift  $\Delta$ , often referred to as Lamb shift in the cavity QED literature [S4], and the Purcell enhanced line width  $\Gamma$  [S5] are then given by

$$\delta := \Delta - i\frac{\Gamma}{2} = \frac{gg^*}{\omega_a - \omega_1 + i\kappa/2}. \quad (\text{S5})$$

Together, they form the complex level shift in Eqs. (3,4) of the main text.

In order to derive spectroscopic observables, one typically considers an external bath Hamiltonian [S6]. The Heisenberg-Langevin equations of motion for the above model then read [S7]

$$\dot{\hat{a}}(t) = -i\left(\omega_1 - i\frac{\kappa}{2}\right)\hat{a}(t) - ig\hat{\sigma}^-(t) - 2\pi i\kappa_R\hat{b}_{\text{in}}(t), \quad (\text{S6})$$

$$\dot{\hat{\sigma}}^-(t) = -i\omega_a\hat{\sigma}^-(t) + ig^*\hat{\sigma}^z(t)\hat{a}(t), \quad (\text{S7})$$

where  $\kappa_R$  is the mode-bath coupling strength, and  $b_{\text{in}}(t)$  the input operator of the bath. The emitted radiation outside the cavity can then be calculated via the input-output relation [S6]

$$\hat{b}_{\text{out}}(t) = \hat{b}_{\text{in}}(t) - i\kappa_R\hat{a}(t). \quad (\text{S8})$$

In the linear spectroscopy regime, we can approximate  $\langle\hat{\sigma}^z(t)\rangle \approx -1$  and  $\langle\hat{\sigma}^z(t)\hat{a}(t)\rangle \approx -\langle\hat{a}(t)\rangle$ , such that the equations of the first order expectation values form a closed system of linear coupled differential equations. The solution for the reflection spectrum defined by  $\langle\hat{b}_{\text{out}}(\omega)\rangle = r(\omega)\langle\hat{b}_{\text{in}}(\omega)\rangle$  is then obtained as

$$r(\omega) = r_{\text{cav}}(\omega) - 2\pi i \frac{|\kappa_R g|^2}{(\omega - \omega_1 + i\kappa/2)^2} \frac{1}{\omega - \omega_a - \frac{gg^*}{\omega - \omega_1 + i\kappa/2}}, \quad (\text{S9})$$

where the empty cavity reflection coefficient is

$$r_{\text{cav}}(\omega) = 1 - 2\pi i \frac{|\kappa_R|^2}{\omega - \omega_1 + i\kappa/2}. \quad (\text{S10})$$

At weak coupling ( $\kappa \gg g$ ) and close to the atomic resonance ( $\kappa \gg \omega - \omega_a$ ), we can approximate the cavity properties as constant on the scale of the light-matter interaction, such that  $1/(\omega - \omega_1 + i\kappa/2) \approx 1/(\omega_a - \omega_1 + i\kappa/2)$ . The spectrum then separates into a constant cavity background and an atomic line as

$$r(\omega) \approx r_{\text{cav}}(\omega_a) - 2\pi i \frac{(\kappa_R^{(\text{int})})^2}{\omega - \omega_a - \Delta + i\Gamma/2}, \quad (\text{S11})$$

which is Eq. (2) in the main text. The resonance modulation depth is given by

$$(\kappa_R^{(\text{int})})^2 = \frac{|\kappa_R g|^2}{(\omega_a - \omega_1 + i\kappa/2)^2}. \quad (\text{S12})$$

The cavity induced Lamb shift  $\Delta$  and Purcell enhanced line width  $\Gamma$  can thus be extracted as line shape parameters from the linear reflection spectrum.

\* dominik.lentrodt@mpi-hd.mpg.de

† joerg.evers@mpi-hd.mpg.de

## II. DETAILS ON THE FEW-MODE EXPANSION AND DIAGONALIZATION

In the main text, we employed a recently-developed few-mode model applicable to general electromagnetic spectral densities [S8] to construct a few-mode expansion of the complex level shift. While the few-mode Hamiltonian used there can in principle be considered a special case of general few-mode system-bath Hamiltonians [S9, S10], the method in [S8] is applicable to absorptive systems and has practical advantages in treating complex resonators. For our purposes, the central advantage is that the requirement of choosing an expansion basis is eliminated if independent and spectrally flat baths are imposed. In the following, we provide details on how this feature allows us to directly relate the resulting mode expansion to the ML pole expansion.

Following the discussion in [S8], the few-mode model Hamiltonian is written as

$$H_{\text{cav}} = \sum_{ij} \omega_{ij} \hat{a}_i^\dagger \hat{a}_j, \quad (\text{S13})$$

where the mode interaction parameters  $\omega_{ij}$  form a real symmetric matrix [S8] and can also be motivated as a basis-transformed version of cross-mode decay terms [S9–S11]. The assumption of spectrally flat and independent baths then results in a Markovian Master equation [S8]

$$\dot{\rho} = -i[H; \rho] + \sum_i \frac{\kappa_i}{2} \left( 2\hat{a}_i \rho \hat{a}_i^\dagger - \hat{a}_i^\dagger \hat{a}_i \rho - \rho \hat{a}_i^\dagger \hat{a}_i \right), \quad (\text{S14})$$

with the real bath coupling parameters  $\kappa_i$ . The two-level system inside the cavity is governed by the light-matter interaction Hamiltonian [S8]

$$H = H_{\text{cav}} + \frac{\omega_a}{2} \hat{\sigma}^z + \sum_i [g_i^* \hat{a}_i \hat{\sigma}^+ + h.c.], \quad (\text{S15})$$

where we used the rotating wave approximation and  $\hbar = 1$ . We note that in [S8], the  $g_i$  are assumed to be real-valued. Here, we consider the option of complex-valued coupling constants, since it provides additional insight into the appearance of multi-mode effects as discussed in Sec. IV.

In the weak coupling limit, upon adiabatic elimination of the cavity modes similarly to the single mode case above, the cavity-induced complex level shift can be written in terms of the mode expansion as

$$\tilde{\delta}(\omega_{\text{test}}) = \underline{g}^\dagger \underline{G} \underline{g}, \quad (\text{S16})$$

$$\underline{G} = \left[ \omega_{\text{test}} \mathbb{I} - \underline{\tilde{H}}_{\text{cav}} \right]^{-1}, \quad (\text{S17})$$

$$\underline{\tilde{H}}_{\text{cav}} = \underline{\omega}_{\text{cav}} - \frac{i}{2} \underline{\kappa}, \quad (\text{S18})$$

where the elements of the vectors and matrices are given by  $(\underline{g})_i = g_i$ ,  $(\underline{\omega}_{\text{cav}})_{ij} = \omega_{ij}$  and  $(\underline{\kappa})_{ij} = \kappa_i \delta_{ij}$ . We note

that  $\underline{G}$  also appears in the expression for the spectral density derived in [S8], where it was used to fit the model parameters. The spectral density is related to the imaginary part of the level shift. The Lamb shift, whose multi-mode features we investigate in the main text, is the real part of the level shift.

The interaction matrix  $\underline{\tilde{H}}_{\text{cav}}$  in the few-mode expansion can be brought to diagonal form via an invertible transformation matrix  $\underline{V}$ . Introducing

$$(\underline{V} \underline{g})_i = \tilde{g}_i, \quad (\text{S19})$$

$$(\underline{V}^{-1} \underline{g}^*)_i = \tilde{g}_i^*, \quad (\text{S20})$$

$$(\underline{V} \underline{\tilde{H}}_{\text{cav}} \underline{V}^{-1})_{ij} = (\tilde{\Omega}_i - i \frac{\tilde{\kappa}_i}{2}) \delta_{ij}, \quad (\text{S21})$$

the few-mode expansion Eq. (S16) can be written as

$$\tilde{\delta}(\omega_{\text{test}}) = \underline{g}^\dagger \underline{G} \underline{g} = \sum_i \frac{\tilde{g}_i^* \tilde{g}_i}{\omega_{\text{test}} - \tilde{\Omega}_i + i \frac{\tilde{\kappa}_i}{2}}. \quad (\text{S22})$$

This expression is now of the same form as the Mittag-Leffler pole expansion (see also Eq. (S28) below) and we can read off the poles and residues in terms of the diagonalized mode frequencies and couplings as

$$\tilde{\omega}_{\text{pole}, i} = \tilde{\Omega}_i - i \frac{\tilde{\kappa}_i}{2}, \quad (\text{S23})$$

$$r_i = \tilde{g}_i^* \tilde{g}_i. \quad (\text{S24})$$

We note that the transformation  $\underline{V}$  is typically not unitary for the lossy systems that we are considering, such that applying it on an operator level yields modified commutation relations and  $\tilde{g}_i$  is generally not equal to  $\tilde{g}_i$ . The ML pole expansion thus corresponds to a non-hermitian diagonal basis, whose associated field operators do not necessarily feature standard bosonic commutation relations (see [S12] for a the related quantization of quasmodes).

The assumption of no exceptional points enters since otherwise the few-mode interaction matrix  $\underline{\tilde{H}}_{\text{cav}}$  is not diagonalizable by an invertible matrix. On the pole expansion side, we incorporated the same assumption by only including simple pole terms, to achieve self-consistency.

## III. MITTAG-LEFFLER EXPANSION OF THE COMPLEX LEVEL SHIFT

Next to the few-mode expansion, the cavity-induced energy shift and line broadening can alternatively be expressed via the classical electromagnetic Green's tensor  $\mathbf{G}$  of the cavity environment as [S13–S15]

$$\delta = -\mu_0 \omega_a^2 \mathbf{d}^* \cdot \mathbf{G}(\mathbf{r}_a, \mathbf{r}_a, \omega_a) \cdot \mathbf{d}, \quad (\text{S25})$$

where  $\mathbf{r}_a$  is the atom's position and  $\mathbf{d}$  its transition dipole moment. This expression applies rather generally for dipole transitions in absorptive dielectric environments [S14], but does not directly provide insight into the modal

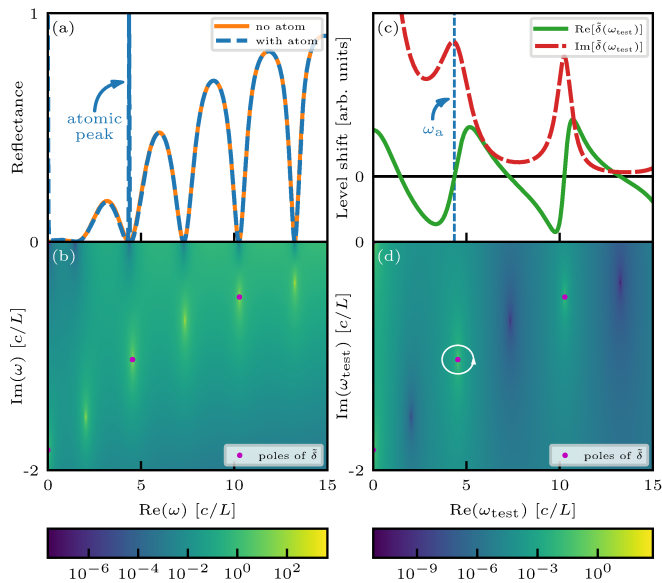


FIG. S1. Illustration of the Mittag-Leffler expansion via the reflection spectrum and level shift in the complex frequency plane. (a) Reflectance with and without the atom. (b) Corresponding spectrum without the atom in the complex frequency plane. (c) Lamb shift and Purcell enhanced line width as a function of frequency. (d) Absolute value squared of the level shift in the complex frequency plane. Poles are marked in magenta. Note that the empty-cavity reflection has additional poles, which the atom does not couple to due to symmetry. An exemplary contour for the determination of the pole residue is shown in (d) as white circle.

structure of the resonator, which is instead encoded in the few-mode or pole expansion as explained in the main text.

However, the Green's function is useful in this context as it provides access to the pole expansion without the need for a fitting routine. To this end, we introduce a test frequency  $\omega_{\text{test}}$  and generalize the complex level shift to a frequency-dependent quantity (indicated by the tilde) as

$$\tilde{\delta}(\omega_{\text{test}}) = -\frac{\mu_0 \omega_a^2}{\hbar} \mathbf{d}^* \cdot \mathbf{G}(\mathbf{r}_a, \mathbf{r}_a, \omega_{\text{test}}) \cdot \mathbf{d}. \quad (\text{S26})$$

Note that the  $\omega_a^2$  prefactor is kept constant, since we are only interested in characterizing the modal structure encoded in the Green's function. This choice is also important to achieve consistency with quantum optical few-mode models discussed in Sec. II, where the  $g_i$ -couplings implicitly depend on  $\omega_a$  in the same fashion [S10]. The generalization allows us to perform a Mittag-Leffler pole expansion along the frequency axis [S16]

$$\tilde{\delta}(\omega_{\text{test}}) = \tilde{\delta}(0) + \sum_i \left[ \frac{r_i}{\tilde{\omega}_{\text{pole},i}} + \frac{r_i}{\omega_{\text{test}} - \tilde{\omega}_{\text{pole},i}} \right], \quad (\text{S27})$$

where we again assume that the system does not contain exceptional points [S17, S18], such that only simple poles are present.

In practice, this expansion can be obtained numerically by finding the poles  $\tilde{\omega}_{\text{pole},i}$  of the Green's function in the complex frequency plane and subsequent evaluation of their residue  $r_i$  by a line integral around the pole, as illustrated in Fig. S1(d) [S16]. For the cases considered in the paper, we find that the constant term converges to zero, such that we can consider the simpler expansion

$$\tilde{\delta}(\omega_{\text{test}}) = \sum_i \frac{r_i}{\omega_{\text{test}} - \tilde{\omega}_{\text{pole},i}}. \quad (\text{S28})$$

This property can also be understood as a general feature of certain Green's functions [S19, S20]. For more advanced numerical schemes we refer to [S20, S21].

The physical level shift is then given by

$$\delta = \tilde{\delta}(\omega_a) = \sum_i \frac{r_i}{\omega_a - \tilde{\omega}_{\text{pole},i}}. \quad (\text{S29})$$

We note that in the frequency-dependent generalized level shift  $\tilde{\delta}(\omega_a)$ , the residues also acquire a dependence on  $\omega_a$ , i.e.,  $r_i = r_i(\omega_a)$ .

An illustration of the reflection spectrum and the complex level shift in the complex frequency plane is given in Fig. S1, together with a contour line around a pole illustrating the numerical method for finding the Mittag-Leffler expansion. The close correspondence between the poles in the complex level shift and the poles in the complex reflection spectrum is clearly visible.

We note that such expansion techniques of the Green's function and other observables are widely used in quasi-mode and scattering theory (see e.g. [S12, S20, S22–S25]). A central novelty of our approach in this context is the relation to few-mode expansions and the resulting interpretation of quantum optical multi-mode effects. The significance of this question already becomes clear if one notes that the ML expansion is unique and independent of a modal basis choice. In contrast, an entire zoo of generalized mode quantization schemes exists on the quantum optical model side [S8–S10, S12, S20, S26–S32] (and even approaches beyond the mode concept [S33–S36]), not least motivated by the desire to circumvent limitations associated with the original Gardiner-Collet Hamiltonian [S6, S10, S12]. Our scheme draws connections between the two sides and allows for a simple categorization of quantum optical multi-mode effects.

#### IV. INTERPRETATION OF MULTI-MODE EFFECTS IN TERMS OF COUPLINGS IN QUANTUM MODELS

In this supplement, we demonstrate how the classification of the different multi-mode effects arises precisely from the view-point of the few-mode quantum models.

To this end, we specialize the derivation in Sec. II to the case of a diagonal interaction matrix  $\omega_{ij}$  in Eq. (S13). This case corresponds to the usual multi-mode extensions of the Jaynes-Cummings model, which do not consider

direct interactions between the modes [S8, S31] or the analogous cross-mode decay terms in [S9–S11]. In this case,  $\underline{H}_{\text{cav}}$  naturally is of diagonal form, and the complex level shift reduces to

$$\tilde{\delta}^{(\text{diag})}(\omega_{\text{test}}) = \sum_i \frac{g_i^\dagger g_i}{\omega_{\text{test}} - \omega_{ii} + i\frac{\kappa_i}{2}}. \quad (\text{S30})$$

In this special case, the few-mode expansion is therefore identical to an ML expansion and the residues are *real-valued*.

As a result, we can directly attribute the appearance of complex-valued residues in the ML expansion to the non-diagonal elements of the mode coupling matrix  $\omega_{ij}$  in Eq. (S13).

A residue with a relevant imaginary contribution may already appear in the case where a single pole is sufficient to achieve convergence in the ML expansion. In terms of the quantum optical few-mode models, this corresponds to the case in which a cavity degree of freedom (i.e., a single element of the non-hermitian diagonal basis) is sufficient, albeit in the presence of significant interaction between multiple “bare” cavity modes. In the main text, we denoted this case as the *complex-residue effect*, which is illustrated in Fig. 2 of the main text. Effectively, it mixes the cavity-induced Lamb shift  $\Delta$  and the superradiant enhancement of the line width  $\Gamma$  in the complex level shift  $\delta$ .

Further multi-mode effects may arise if multiple poles are required for the convergence of the ML expansion, which we denote as *multi-pole effects*. In this case, multiple cavity degrees of freedom (i.e., multiple elements of the non-hermitian diagonal basis) are required for convergence on the level of the few-mode model.

Both complex-residue and multi-pole effects are *multi-mode effects*, since they require multiple modes in the few-mode expansion and cannot be explained by the standard single mode Jaynes-Cummings model.

These results show that the features of the Mittag-Leffler pole expansion used in the main text indeed certify multi-mode effects in the light-matter interaction. The above viewpoint of quantum optical few-mode theory further provides an interpretation for the origin of the two types of resonant multi-mode effects that we identify.

For completeness, we note that for some systems, poles at negative real frequency contribute to the Mittag-Leffler expansion. On the level of the pole expansion, this feature does not make a difference. On the level of quantum optical models, a fully consistent treatment would be to include counter-rotating terms in the system-bath coupling [S10]. This, however, would not affect the classification and interpretation of the multi-mode effects in terms of the ML expansion discussed in the main text.

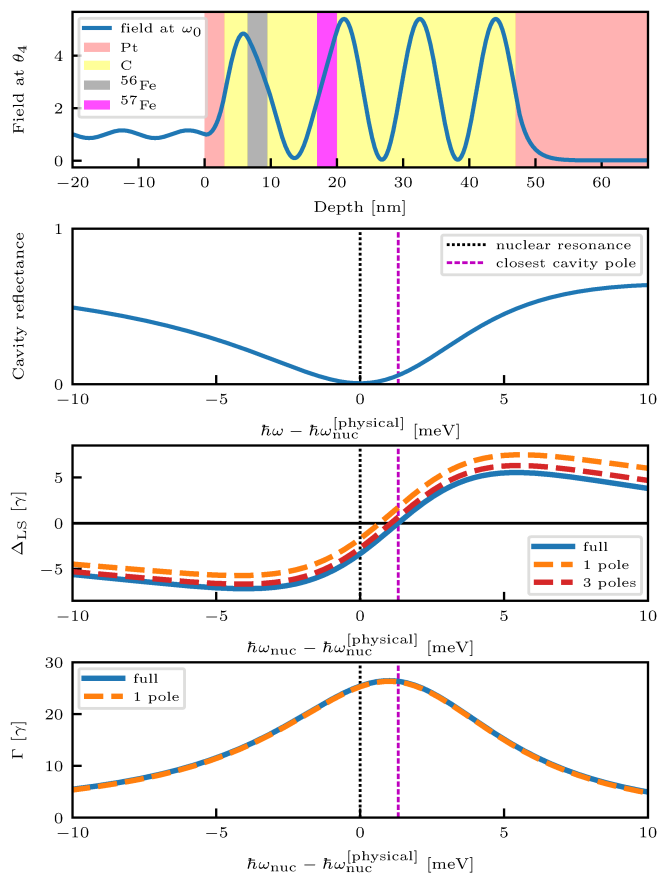


FIG. S2. Multi-mode effects in the x-ray cavity considered in Fig. 4 of the main text. The x-ray incidence angle is chosen such that the fourth mode minimum lies on resonance. (a) Cavity structure (see legend) and off-resonant cavity-field strength at the resonance frequency  $\omega_{\text{nuc}}^{[\text{physical}]} = 14.4$  keV. (b) Off-resonant cavity reflectance as a function of energy. Note that the incidence angle is chosen such that the first reflection minimum lies on resonance. The real part of the main cavity pole is shifted with respect to the reflection minimum, indicating that this cavity features off-resonant multi-mode effects. (c, d) cavity induced Lamb shift and Purcell enhanced line width, respectively, as a function of nuclear transition frequency relative to its physical value. We see that a ML expansion containing only the main pole already suffices to reproduce the line width, while few modes are required for convergence in the Lamb shift. Thus, the cavity does feature resonant multi-mode effects, in addition to the off-resonant ones.

## V. INTERPRETATION OF OFF-RESONANT MULTI-MODE EFFECTS IN TERMS OF BACKGROUND SCATTERING

For the above few-mode model, one can in principle apply the input-output formalism [S7] to obtain spectroscopic observables such as the empty cavity reflection coefficient (that is without the atom). However, the result will not be exact due to the truncation of the mode expansion. For isolated resonances, the latter can still be

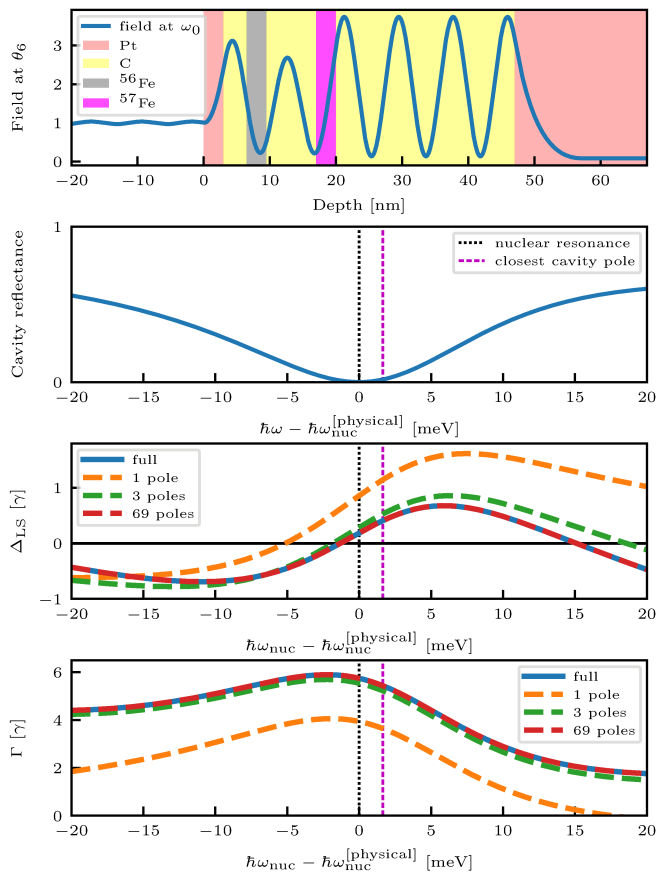


FIG. S3. This figure is analogous to Fig. S2, but with the x-ray incidence angle chosen such that the sixth mode minimum lies on resonance. In this case, we observe strong resonant multi-mode effects for both  $\Delta$  and  $\Gamma$ , including multi-pole convergence and a significantly complex residue of the main pole. These results show that the inversion of the collective Lamb shift reported in Fig. 4 of the main text indeed is a multi-mode effect.

a good representation of the reflection. For the case of overlapping resonances, however, a background scattering contribution is required, as shown in [S10]. In particular if a fitting procedure as the one in [S8] is employed, the bath modes will generally not even be the asymptotic scattering degrees of freedom.

We note that this does not invalidate the approach for the purpose of computing the system dynamics in the cavity. Indeed, the input-output scattering can be translated to the full scattering result via the background scattering contribution [S10]. Interestingly, since the latter is an off-resonant cavity property, it can still be significant even if the few-mode expansion of the resonant dynamics is already well converged.

In the present context, the off-resonant multi-mode effects can straightforwardly be identified as arising from non-negligible background scattering contributions. The interpretation as a separate phenomenon to the two resonant multi-mode effects therefore also directly maps to

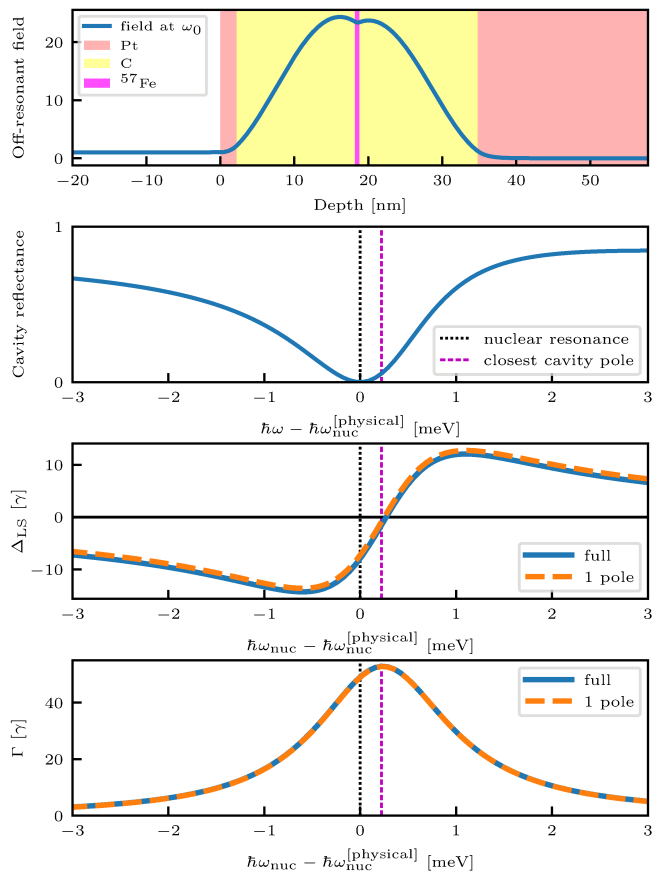


FIG. S4. This figure is analogous to Fig. S2, but for the cavity structure considered in the experiment reported in [S37]. We see that resonant multi-mode effects are negligible. The non-zero Lamb shift at the rocking minimum is explained by an off-resonant multi-mode shift.

quantum optical few-mode models.

## VI. MULTI-MODE EFFECTS IN X-RAY CAVITY QED WITH MÖSSBAUER NUCLEI

In the main text, we show that multi-mode effects can be used to invert the collective Lamb shift in x-ray cavity QED with Mössbauer nuclei. In the following, we illustrate this example further, and in particular show the contributions of the different multi-mode effects to the Lamb shift inversion.

Fig. S2 shows results for the cavity considered in the main text, with the x-ray angle of incidence chosen such that the reflection minimum of the fourth cavity mode is on resonance with the nuclei. Panel (a) shows the cavity structure together with the resulting field intensity, off-resonant with the nuclei. (b) shows the reflectance, which by design has a minimum at the nuclear resonance. The panel further shows the position of the closest main cavity pole from the ML expansion. Its shift relative to the reflection minimum indicates the presence of off-resonant

multi-mode effects. Panels (c,d) show the cavity-induced Lamb shift and the Purcell enhanced line width. It can be seen that the line width is already converged upon inclusion of the single main pole contribution. In contrast, few poles are required for a converged Lamb shift. We thus find that the cavity also features resonant multi-mode effects, however, with only small line shape modifications, and less pronounced than the off-resonant multi-mode effects.

Fig. S3 shows corresponding results for an x-ray incidence angle chosen such that the reflection minimum of the sixth mode is on resonance. In this case, in addition to an off-resonant multi-mode shift, strong resonant multi-mode effects occur. Both, the line width broadening and the cavity Lamb shift require the summation of multiple poles to achieve convergence. Furthermore, sizeable line-shape distortions appear, indicating the presence of complex-residue and multi-pole effects. The res-

onant multi-mode effects are strong enough to outweigh the off-resonant multi-mode effects, such that in total a reversed shift is obtained. In particular, the imaginary part of the main pole's residue (sixth pole, orange dashed line) majorly contributes to the inversion. The contributions of higher modes act to reduce the positive shift again, but a significant shift remains at the minimum even when the result is fully converged. This clearly shows that the Lamb shift inversion can be attributed to the resonant multi-mode effects.

Finally, Fig. S4 summarizes the results of an analogous investigation for the cavity structure considered in the experiment reported in [S37]. It can be seen that resonant multi-mode effects are negligible in this case. Instead, the non-zero Lamb shift at the rocking minimum, which is incompatible with single-mode models, is identified as an off-resonant multi-mode shift.

- 
- [S1] E. T. Jaynes and F. W. Cummings, *Comparison of quantum and semiclassical radiation theories with application to the beam maser*, Proc. IEEE **51**, 89 (1963).
- [S2] S. Haroche and J. M. Raimond, *Exploring the Quantum: Atoms, Cavities, and Photons* (Oxford Univ. Press, Oxford, 2006).
- [S3] K. P. Heeg and J. Evers, *X-ray quantum optics with mössbauer nuclei embedded in thin-film cavities*, Phys. Rev. A **88**, 043828 (2013).
- [S4] M. F. Limonov, M. V. Rybin, A. N. Poddubny, and Y. S. Kivshar, *Fano resonances in photonics*, Nat. Phot. **11**, 543 EP (2017).
- [S5] E. M. Purcell, *Spontaneous emission probabilities at radio frequencies*, Phys. Rev. **69**, 681 (1946).
- [S6] C. W. Gardiner and M. J. Collett, *Input and output in damped quantum systems: Quantum stochastic differential equations and the master equation*, Phys. Rev. A **31**, 3761 (1985).
- [S7] C. W. Gardiner and P. Zoller, *Quantum noise* (Springer, Heidelberg, 2004).
- [S8] I. Medina, F. J. García-Vidal, A. I. Fernández-Domínguez, and J. Feist, *Few-mode field quantization of arbitrary electromagnetic spectral densities*, Phys. Rev. Lett. **126**, 093601 (2021).
- [S9] C. Viviescas and G. Hackenbroich, *Field quantization for open optical cavities*, Phys. Rev. A **67**, 013805 (2003).
- [S10] D. Lentrodt and J. Evers, *Ab initio few-mode theory for quantum potential scattering problems*, Phys. Rev. X **10**, 011008 (2020).
- [S11] G. Hackenbroich, C. Viviescas, and F. Haake, *Field quantization for chaotic resonators with overlapping modes*, Phys. Rev. Lett. **89**, 083902 (2002).
- [S12] S. Franke, S. Hughes, M. K. Dezfouli, P. T. Kristensen, K. Busch, A. Knorr, and M. Richter, *Quantization of quasinormal modes for open cavities and plasmonic cavity quantum electrodynamics*, Phys. Rev. Lett. **122**, 213901 (2019).
- [S13] H. T. Dung, L. Knöll, and D.-G. Welsch, *Spontaneous decay in the presence of dispersing and absorbing bod-*  
*ies: General theory and application to a spherical cavity*, Phys. Rev. A **62**, 053804 (2000).
- [S14] S. Scheel and S. Y. Buhmann, *Macroscopic quantum electrodynamics - concepts and applications*, Acta Phys. Slovaca **58**, 675 (2008).
- [S15] A. Asenjo-Garcia, J. D. Hood, D. E. Chang, and H. J. Kimble, *Atom-light interactions in quasi-one-dimensional nanostructures: A green's-function perspective*, Phys. Rev. A **95**, 033818 (2017).
- [S16] M. R. Spiegel, S. Lipschutz, J. J. Schiller, and D. Spellman, *Schaum's Outline of Complex Variables, 2ed*, Schaum's Outline Series (McGraw-Hill Education, 2009).
- [S17] M.-A. Miri and A. Alù, *Exceptional points in optics and photonics*, Science **363** (2019), 10.1126/science.aar7709.
- [S18] S. K. Özdemir, S. Rotter, F. Nori, and L. Yang, *Parity-time symmetry and exceptional points in photonics*, Nature Materials **18**, 783 (2019).
- [S19] J. Defrance and T. Weiss, *On the pole expansion of electromagnetic fields*, Opt. Express **28**, 32363 (2020).
- [S20] P. Lalanne, W. Yan, K. Vynck, C. Sauvan, and J.-P. Hugonin, *Light interaction with photonic and plasmonic resonances*, Laser & Photonics Reviews **12**, 1700113 (2018).
- [S21] T. Wu, D. Arrivault, M. Duruflé, A. Gras, F. Binkowski, S. Burger, W. Yan, and P. Lalanne, *Efficient hybrid method for the modal analysis of optical microcavities and nanoresonators*, J. Opt. Soc. Am. A **38**, 1224 (2021).
- [S22] F. Binkowski, F. Betz, R. Colom, M. Hammer-schmidt, L. Zschiedrich, and S. Burger, *Quasinormal mode expansion of optical far-field quantities*, Phys. Rev. B **102**, 035432 (2020).
- [S23] H. Zhang and O. D. Miller, *Quasinormal coupled mode theory*, (2020), arXiv:2010.08650 [physics.optics].
- [S24] F. Alpeggiani, N. Parappurath, E. Verhagen, and L. Kuipers, *Quasinormal-mode expansion of the scattering matrix*, Phys. Rev. X **7**, 021035 (2017).
- [S25] M. Benzaouia, J. D. Joannopoulos, S. G. Johnson, and

- A. Karalis, Quasi-normal mode theory enforcing fundamental constraints for truncated expansions, (2021), arXiv:2105.01749 [physics.app-ph].
- [S26] B. M. Garraway, *Nonperturbative decay of an atomic system in a cavity*, Phys. Rev. A **55**, 2290 (1997).
- [S27] B. M. Garraway, *Decay of an atom coupled strongly to a reservoir*, Phys. Rev. A **55**, 4636 (1997).
- [S28] D. Tamascelli, A. Smirne, S. F. Huelga, and M. B. Plenio, *Nonperturbative treatment of non-markovian dynamics of open quantum systems*, Phys. Rev. Lett. **120**, 030402 (2018).
- [S29] P. T. Kristensen and S. Hughes, *Modes and Mode Volumes of Leaky Optical Cavities and Plasmonic Nanoresonators*, ACS Photonics **1**, 2 (2014).
- [S30] E. S. C. Ching, P. T. Leung, A. Maassen van den Brink, W. M. Suen, S. S. Tong, and K. Young, *Quasinormal-mode expansion for waves in open systems*, Rev. Mod. Phys. **70**, 1545 (1998).
- [S31] S. Franke, M. Richter, J. Ren, A. Knorr, and S. Hughes, *Quantized quasinormal-mode description of nonlinear cavity-qed effects from coupled resonators with a fano-like resonance*, Phys. Rev. Research **2**, 033456 (2020).
- [S32] C. Viviescas and G. Hackenbroich, *Quantum theory of multimode fields: applications to optical resonators*, J. Opt. B **6**, 211 (2004).
- [S33] D. O. Krimer, M. Liertzer, S. Rotter, and H. E. Türeci, *Route from spontaneous decay to complex multimode dynamics in cavity QED*, Phys. Rev. A **89**, 033820 (2014).
- [S34] M. Malekakhlagh, A. Petrescu, and H. E. Türeci, *Cutoff-free circuit quantum electrodynamics*, Phys. Rev. Lett. **119**, 073601 (2017).
- [S35] A. Strathearn, P. Kirton, D. Kilda, J. Keeling, and B. W. Lovett, *Efficient non-markovian quantum dynamics using time-evolving matrix product operators*, Nature Communications **9**, 3322 (2018).
- [S36] D. Gribben, A. Strathearn, J. Iles-Smith, D. Kilda, A. Nazir, B. W. Lovett, and P. Kirton, *Exact quantum dynamics in structured environments*, Phys. Rev. Research **2**, 013265 (2020).
- [S37] R. Röhlsberger, K. Schlage, B. Sahoo, S. Couet, and R. Ruffer, *Collective lamb shift in single-photon super-radiance*, Science **328**, 1248 (2010).